Optics Letters

Temperature dependence mitigation in stationary Fourier-transform on-chip spectrometers

Alaine Herrero-Bermello,[1,*] Aitor V. Velasco,[1] Hugh Podmore,[2] Pavel Cheben,[3] Jens H. Schmid,[3] Siegfried Janz,[3] María L. Calvo,[4] Dan-Xia Xu,[3] Alan Scott,[5] and Pedro Corredera[1]

[1]*Institute of Optics, Spanish National Research Council, Madrid 28006, Spain*
[2]*Department of Physics and Astronomy, York University, Toronto, Ontario M3J 1P3, Canada*
[3]*National Research Council Canada, Ottawa, Ontario K1A 0R6, Canada*
[4]*Faculty of Physics, Complutense University of Madrid, Madrid 28040, Spain*
[5]*Honeywell Aerospace, Kanata, Ontario, Canada*
**Corresponding author: alaine.herrero@csic.es*

Received 24 March 2017; revised 28 April 2017; accepted 28 April 2017; posted 4 May 2017 (Doc. ID 291293); published 0 MONTH 0000

We present two techniques for mitigating the effects of temperature drifts in waveguide spatial heterodyne Fourier-transform on-chip spectrometers. In high-resolution devices, large optical path length differences result in an increased sensitivity to temperature variations and impose stringent requirements on the thermal stabilization system. In order to overcome this limitation, here we experimentally demonstrate two new temperature mitigation techniques based on a temperature-sensitive calibration and phase error correction. The spectrometer chip under analysis comprises an array of 32 Mach–Zehnder interferometers fabricated on a silicon-on-insulator platform. The optical path delays are implemented as microphotonic spirals of linearly increasing length up to 3.779 cm, yielding a spectral resolution of 17 pm. We demonstrate that the degradation in retrieved spectra caused by temperature drift is effectively eliminated by temperature-sensitive calibration and phase error correction.

OCIS codes: (130.0130) Integrated optics; (300.0300) Spectroscopy.

https://doi.org/10.1364/OL.99.099999

Integrated spectrometers are sought after for a wide range of applications, such as optical communications, health diagnostics, biological and environmental sensing, and remote sensing from microsatellites [1,2], to name a few. Integrated spectrometers based on arrayed waveguide gratings [3], Bragg gratings [4], waveguide echelle and concave gratings [5,6], and cascaded microring resonators [7,8] can achieve subnanometer spectral resolutions and compact chip sizes. However, the optical throughput (*étendue*) of these devices is fundamentally limited by the need for a single-mode input waveguide. On the contrary, spatial heterodyne Fourier-transform (SHFT) spectrometers can provide a substantially larger *étendue* due to the possibility of multiple input waveguide apertures [9]. In an SHFT system, multiple interferometric measurements are performed in parallel using an array of interferometers, each with a different optical path length difference (OPD) [10]. The input spectrum is calculated by the Fourier transform (FT) of the stationary spatial interferogram, which can be captured by a detector array in a single shot.

SHFT spectrometers have been successfully implemented on silicon-on-insulator (SOI) platforms [9]. The high refractive index contrast of SOI provides a high modal confinement with a correspondingly reduced bend radius, which ultimately allows a larger spectral resolution on a smaller chip footprint. The SHFT spectrometer can be implemented on an SOI platform as an array of N waveguide Mach–Zehnder interferometers (MZIs) [9]. In such a configuration, the spectral resolution ($\delta\lambda$) is determined by the OPD of the most unbalanced interferometer while the free spectral range (FSR) is set by the numbers of interferometers (N) [9,11]:

$$\delta\lambda = \frac{\lambda_0^2}{\Delta L_{\max} n_g}, \tag{1}$$

$$\mathrm{FSR} = \delta\lambda \frac{N}{2}, \tag{2}$$

where λ_0 is the device central wavelength, $\Delta L_{\max}$ is the maximum MZI geometrical path difference, and n_g is the waveguide group index. For an arbitrary input signal, all the interferometer outputs (each corresponding to a different optical path difference) are measured simultaneously, resulting in a stationary wavelength-dependent spatial interferogram $\boldsymbol{I(x)_i}$. The relation between the input spectral density $B(\bar{\sigma})$ and the output interferogram within the FSR of the device is given by [9]

$$I(x_i) = \int_0^{\mathrm{FSR}} B(\bar{\sigma}) \cos(2\pi\bar{\sigma}x_i) \mathrm{d}\bar{\sigma}, \tag{3}$$

where $\bar{\sigma} = \sigma - \sigma_L$ is the shifted wavenumber, relative to the Littrow wavenumber σ_L [12] at which maxima of the MZI responses are aligned, and x_i is the path delay of the ith MZI. This relation is unambiguous for an ideal device without phase errors, enabling the source spectrum to be retrieved by the Fourier cosine transform.

However, in fabricated devices, two main deviations from the ideal behavior are present. Interferogram visibility variations are produced by uneven propagation losses in waveguides across the array. As the waveguide loss imbalance progressively increases with optical path difference between the MZI arms across the array, interferogram visibility is correspondingly reduced. This effect can be readily compensated by normalization techniques [12]. Furthermore, fluctuations in fabricated waveguide properties, particularly the waveguide width, produce fluctuations of the waveguide effective index, resulting in random phase errors in the MZI transmittance functions. Therefore, the phase alignment condition of the Littrow wavenumber and orthogonality of the FT transformation base are not guaranteed, rendering Eq. (3) inadequate for practical spectral retrieval.

To compensate for these errors, the use of active elements (heaters) [11] was proposed. Alternatively, a fully passive spectral retrieval algorithm based on a calibration matrix was developed [12]. Nevertheless, in order to ensure that the calibration matrix is correctly implemented, MZI transmittance functions must remain invariant between the calibration and the measurement steps. The thermal dependence of Si-wire waveguides hampers this requirement [13], as temperature variations change the waveguide effective index and, therefore, the OPD of each interferometer. This alters the MZI transmittance functions, producing additional phase errors. For example, the thermooptic coeficients of Si-wire waveguides used in the SHFT in [12], dn_{eff}/dT, are $1.8 \cdot 10^{-4}\ \mathrm{K}^{-1}$ and $1.2 \cdot 10^{-4}\ \mathrm{K}^{-1}$ for TE and TM polarizations, respectively, at a wavelength of 1.55 μm [13]. Since the thermal-induced phase shift increases with the interferometric delay, this imposes stringent requirements on the thermal stabilization, particularly for devices with high spectral resolution. Here we present two novel spectral retrieval methods, based on temperature-sensitive calibration and phase error correction to mitigate SHFT temperature dependence. The technique is implemented on an SHFT device with a resolution of 17 pm at a central wavelength of 1550 nm, with a compact footprint of 23 mm^2.

Our first algorithm is based on the measurement of multiple calibration matrices ($\boldsymbol{C_j}$) of the same device at different temperatures (T_j), followed by the automated selection of the appropriate matrix for each particular spectral retrieval. The number of required calibration matrices depends on the relation between the maximum temperature range for a specific application and the minimum temperature change, which provides correct spectral retrieval. The output interferogram can be expressed as $\boldsymbol{I(x_i, T_j, \lambda_k) = B(\lambda_k) \times C_j}$, where λ_k are specific wavelengths within the FSR of the device. In each calibration matrix $\boldsymbol{C_j}$, the transmittance function of each MZI is sampled at M typically equidistant wavelengths with a narrowband tunable laser within the FSR of the device. Each matrix hence comprises N rows, which represent the normalized power of the output interferogram for each wavelength, and M columns, corresponding to the spectral response of each MZI. In an ideal scenario, the source spectrum can be obtained by multiplying the interferogram by the inverse of the transformation matrix. When the transformation base is not orthogonal (e.g., in the presence of phase errors), the calibration matrix is not invertible and its pseudoinverse is used instead.

For the correct selection of the temperature-dependent calibration matrix, an auxiliary temperature measurement is required. This step can be directly performed with a high-precision measurement of the chip temperature (T_{aux}). The calibration matrix selected for the spectral retrieval algorithm is then the matrix, $\boldsymbol{C_j}$, obtained at the temperature T_j nearest to T_{aux}. Alternatively, the output interferogram ($\boldsymbol{I_{\mathrm{aux}}}$) of a reference input signal with a known spectrum ($\boldsymbol{B_{\mathrm{ref}}}$) can be used for accurate temperature determination. In this case, the appropriate calibration matrix is selected by minimizing the following expression:

$$\sum_{i=1}^{N} |I_{\mathrm{aux}} - B_{\mathrm{ref}} \times C_j|. \quad \textbf{(4)}$$

Our second algorithm utilizes amplitude and phase error correction for narrowband signals. Each MZI's transmittance function in the calibration matrix is (mathematically) normalized, shifted, and aligned, obtaining an aligned matrix $\boldsymbol{C'_j}$ and a phase shift vector $\boldsymbol{\Delta\lambda}$:

$$C'_j(x_i, \lambda_k) = C_j(x_i, \lambda_k - \Delta\lambda(x_i)). \quad \textbf{(5)}$$

By applying this vector to the output interferogram to be analyzed, a corrected interferogram $\boldsymbol{I'(x)}_i$ with improved orthogonality and the Littrow condition is obtained. An indetermination arises when applying $\boldsymbol{\Delta\lambda}$, as a given signal level can correspond to either a rising or descending flank of the MZI transmittance function. This issue can be solved in the particular case of narrowband input spectra by measuring the output interferogram at two close temperatures (T and $T + \Delta T$). By analyzing the effect of small temperature changes in the output signal levels, the indetermination is resolved.

Both algorithms were demonstrated on an SHFT microspectrometer comprising an array of 32 silicon waveguide MZIs with a reference straight arm of constant length and a microphotonic spiral arm with linearly increasing length (Fig. 1). The high index contrast of the SOI platform enables

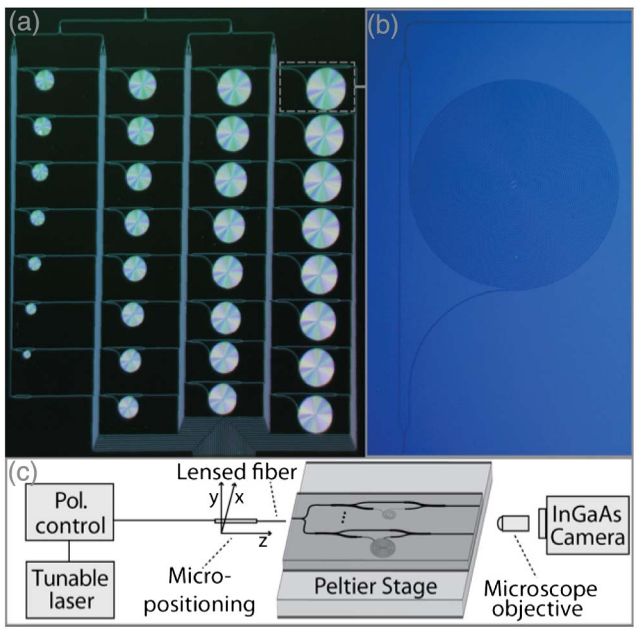

Fig. 1. (a) Optical micrograph of the fabricated spatial heterodyne Fourier-transform spectrometer chip with spiral silicon wire waveguides, and (b) details of the most unbalanced Mach–Zehnder interferometer. (c) Schematic description of the measurement setup.

fabrication of tightly coiled spirals. Here we implemented a maximum length difference of 3.779 cm in a spiral diameter of only 490 µm. To ensure single-mode operation and negligible bend losses, 450 nm wide × 260 nm thick Si-wire waveguides with a minimum bend radius of 5 µm were used. Propagation losses of −4 dB/cm were measured, with bending losses of −1.7 dB/cm in the spiral sections.

These design parameters result in a theoretical spectral resolution of 14.5 pm and an FSR of 0.23 nm in a compact device footprint of 23 mm^2. Efficient subwavelength grating edge couplers [14] integrated on the chip were used for fiber-chip coupling, while at the same time reducing the Fabry–Perot effect by minimizing the reflectivity at the facets.

The device was fabricated on SOI wafers with 260 nm thick silicon and 2 µm buried oxide. The waveguides were defined in a single patterning step by electron beam lithography using hydrogen silsesquioxane resist. Inductively coupled plasma reactive ion etching was used to transfer the resist pattern into the silicon layer.

The fabricated device was characterized using a high-resolution tunable semiconductor laser over the spectral range of 1550–1550.6 nm, with a wavelength step of 0.5 pm. A Peltier stage was used for thermal stabilization of the chip, and a TE-polarization state was selected through an external polarization controller [Fig. 1(c)]. Output light from the MZIs was collimated by a microscope objective and captured in a single shot with a high-sensitivity InGaAs camera.

For the microspectrometer under analysis, the TE-polarization calibration matrix was measured at three different temperatures ($T_1 = 22.4$°C, $T_2 = 22.5$°C, and $T_3 = 22.7$°C). Room temperature was maintained at 22.4°C. The responses of three interferometers (24, 27, and 32) were removed from the matrix due to a low signal-to-noise ratio caused by some defective waveguides. Due to the exclusion of the last MZI (#32, with the maximum imbalance), the maximum length difference is reduced to 3.658 cm, leading to a theoretical resolution of 15 pm. A revised theoretical FSR of 0.22 nm is estimated for this set of 29 interferometers. Figure 2 shows the calibration maps for these three specific temperatures, without amplitude or phase corrections. The visibility reduction can be observed along the horizontal axis (MZI number), while along the vertical axis (wavelength) the misalignments of the transmittance functions of different MZIs due to phase errors are noticed.

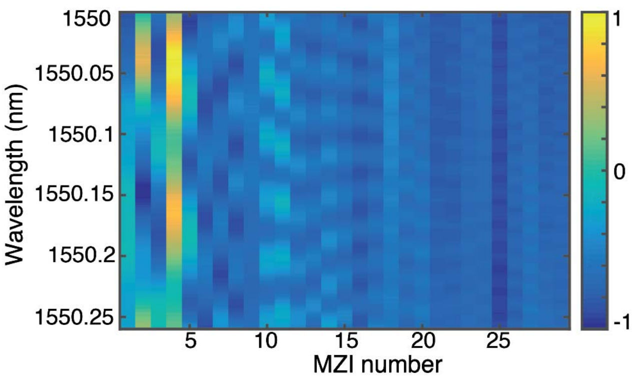

Fig. 2. Experimental characterization of the spectral response of each interferometer in a 0.26 nm FSR for three different temperatures ($T_1 < T_2 < T_3$).

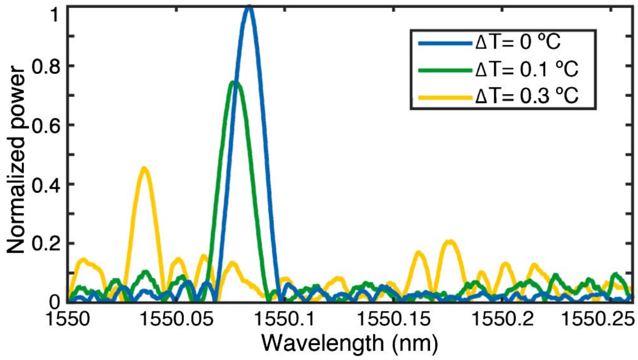

Fig. 3. Spectral retrievals of a first monochromatic input signal measured at 22.4°C, demonstrating the degradation caused by temperature mismatches (ΔT) between said measurement temperature and the calibration temperature.

In Fig. 3, we show a first experimental spectral retrieval of a monochromatic signal measured at $T = 22.4$°C after selecting the appropriate matrix calibrated at the same temperature ($\Delta T = 0$°C), as well as for several uncorrected temperature mismatches ($\Delta T = 0.1$°C, $\Delta T = 0.3$°C) between calibration and measurement steps. Temperature changes modify the OPD of each interferometer differently. Therefore, a length-dependent displacement of the MZI transmittance functions is produced. As a consequence, the central wavelength is shifted and the sidelobe level increases with the temperature difference. A 6 pm central-wavelength displacement is measured for $\Delta T = 0.1$°C, which corresponds to a 180° phase shift in the output of the longest MZI in the particular device herein described. Significant spectral retrieval deterioration is already found for $\Delta T = 0.3$°C. The relation between ΔT and the described output interferogram changes is proportional to device resolution. An experimental resolution of 17 pm in an FSR of 0.26 nm is demonstrated. This result verifies the circumvention of the stringent temperature control requirements associated with this resolution in previous retrieval algorithms.

Second, in order to correct the nonorthogonality of the Fourier base (phase errors) and the visibility losses (amplitude errors), all the MZI functions in each experimental calibration

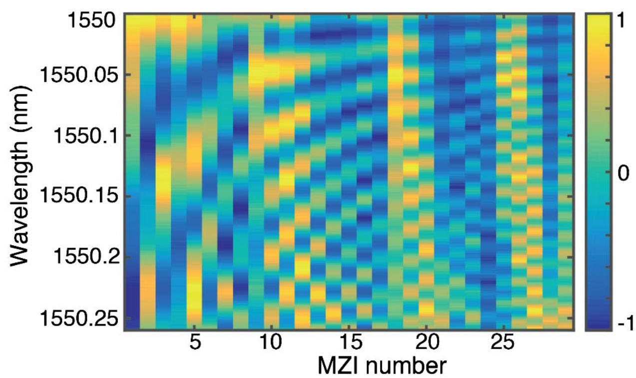

Fig. 4. Calibration map for a temperature of 22.4°C after alignment and shifting of the MZI transmittance functions and normalization. The Littrow condition holds at a wavelength $\lambda_L = 1550$ nm where the transmittance functions of all MZIs are in-phase.

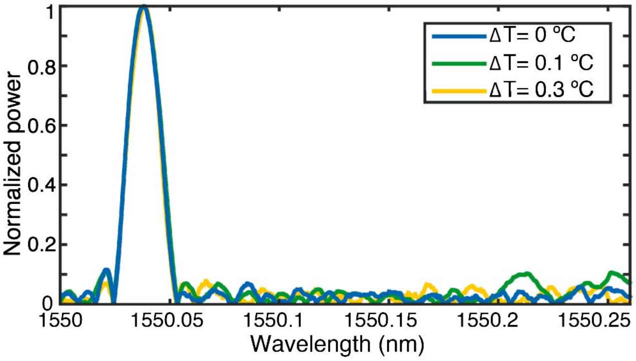

Fig. 5. Spectral retrievals of a second monochromatic input signal using the calibration-based spectral retrieval algorithm after phase and amplitude corrections.

matrix were normalized and aligned to the Littrow wavelength of 1550 nm. The resulting calibration map for a temperature of 22.4°C is shown in Fig. 4. The temperature-dependent phase shift vector, $\Delta\lambda$, was then used to correct the phase errors in the measured interferograms.

Using both of our methods simultaneously, that is selecting the specific calibration matrix and correcting both the phase and amplitude errors, the effects of temperature dependence are compensated and corrected, yielding athermal device behavior. As shown in Fig. 5, the spectral retrieval of a monochromatic source is substantially improved by combining both methods.

In this work, we presented two techniques for compensating the effects of thermal changes in a spatial heterodyne Fourier-transform spectrometer, namely, temperature-dependent calibration matrices and numerical reconstruction of the Littrow condition. These techniques were experimentally implemented on an SHFT device fabricated on an SOI platform. The spectrometer comprises an array of 32 waveguide Mach–Zehnder interferometers with a linearly increasing imbalance across the array, up to 3.779 cm. Spectral retrieval degradation effects caused by the temperature difference between the calibration and the actual spectral measurement were characterized and corrected. A spectral resolution of 17 pm in a 0.22 nm free spectral range was experimentally demonstrated. These results pave the way for the development of athermal high-resolution integrated spectrometers combining hardware and software athermalization techniques for diverse applications ranging from handheld to microsatellite on-chip spectroscopy.

Funding. Ministerio de Economía y Competitividad (MINECO) (FJCI-2014-22836, TEC2015-71127-C2-1-R, TEC2015-71127-C2-2-R); Comunidad de Madrid (S2013/MIT-2790); ~~EURAMET (H2020-MSCA-RISE-2016: SENSIBLE); EMPIR Programme (JRP-i2[illegible]14IND13-PhotInd); National Research Council Canada (NRC); European Union's Horizon 2020 Research and Innovation Programme under Marie Sklodowska-Curie grant (734331).~~

REFERENCES

1. P. Cheben, in *Optical Waveguides: From Theory to Applied Technologies* (CRC Press, 2007), p. 173.
2. J. Wang, J. C. Gille, P. L. Bailey, L. Pan, D. Edwards, and J. R. Drummond, J. Atmos. Sci. **56**, 219 (1999).
3. P. Cheben, J. H. Schmid, A. Delâge, A. Densmore, S. Janz, B. Lamontagne, J. Lapointe, E. Post, P. Waldron, and D.-X. Xu, Opt. Exp. **15**, 2299 (2007).
4. J. H. Song, J. H. Lim, R. K. Kim, K. S. Lee, K. Y. Kim, J. Cho, D. Han, S. Jumg, Y. Oh, and D. H. Jang, IEEE Photon. Technol. Lett. **17**, 2607 (2005).
5. S. Janz, A. Balakrishnan, S. Charbonneau, P. Cheben, M. Cloutier, A. Delâge, K. Dossou, L. Erickson, M. Gao, P. A. Krug, B. Lamontagne, M. Packirisamy, M. Pearson, and D.-X. Xu, IEEE Photon. Technol. Lett. **16**, 503 (2004).
6. A. Malik, M. Muneeb, Y. Shimura, J. Van Campenhout, R. Loo, and G. Roelkens, Appl. Phys. Lett. **103**, 161119 (2013).
7. J. Huang, J. Yang, H. Zhang, J. Zhang, W. Wu, and S. Chang, IEEE Photon. Technol. Lett. **28**, 2677 (2016).
8. Z. Xia, A. A. Eftekhar, M. Soltani, B. Momeni, Q. Li, M. Chamanzar, S. Yegnanarayanan, and A. Adibi, Opt. Express **19**, 12356 (2011).
9. M. Florjańczyk, P. Cheben, S. Janz, A. Scott, B. Solheim, and D.-X. Xu, Opt. Express **15**, 18176 (2007).
10. P. Jacquinot, J. Opt. Soc. Am. **44**, 761 (1954).
11. K. Okamoto, H. Aoyagi, and D. Takada, Opt. Lett. **35**, 2013 (2010).
12. A. V. Velasco, P. Cheben, P. J. Bock, A. Delâge, J. H. Schmid, J. Lapointe, S. Janz, M. L. Calvo, D.-X. Xu, M. Florjańczyk, and M. Vachon, Opt. Lett. **38**, 706 (2013).
13. J. H. Schmid, M. Ibrahim, P. Cheben, J. Lapointe, S. Janz, P. J. Bock, A. Densmore, B. Lamontagne, R. Ma, W. N. Ye, and D.-X. Xu, Opt. Lett. **36**, 2110 (2011).
14. P. Cheben, P. J. Bock, J. H. Schmid, J. Lapointe, S. Janz, D.-X. Xu, A. Densmore, A. Delâge, B. Lamontagne, and T. J. Hall, Opt. Lett. **35**, 2526 (2010).

Queries

1. AU: The funding information for this article has been generated using the information you provided to OSA at the time of article submission. Please check it carefully. If any information needs to be corrected or added, please provide the full name of the funding organization/institution as provided in the CrossRef Open Funder Registry (http://www.crossref.org/fundingdata/registry.html).